



## Article

# Fabrication of Magnetic Catalyst $\text{Fe}_3\text{O}_4\text{-SiO}_2\text{-V}_3$ and Its Application on Lignin Extraction from Corncob in Deep Eutectic Solvent

Maonan Yuan , Zhen Wang \* , Yu Liu and Guihua Yang

State Key Laboratory of Biobased Material and Green Papermaking, School of Environmental Science and Engineering, Qilu University of Technology (Shandong Academy of Sciences), Jinan 250353, China; maonanyuan@126.com (M.Y.); liuy@qlu.edu.cn (Y.L.); ygh@qlu.edu.cn (G.Y.)

\* Correspondence: wangzhenyft@126.com; Tel.: +86-15864791007

**Abstract:**  $\text{Fe}_3\text{O}_4\text{-SiO}_2\text{-V}_3$  was prepared by deposited  $\text{H}_6\text{PMo}_9\text{V}_3\text{O}_{40}$  on  $\text{Fe}_3\text{O}_4\text{-SiO}_2$  and employed as a catalyst to extract lignin from corncob in deep eutectic solvent (choline chloride/lactic acid = 1/10). Batch experiments were conducted in an autoclave under the conditions of 500 kPa, 90–130 °C and 15 h, while the dosage of the catalyst was set as a variable. Results indicated that the catalyst could effectively improve the qualities of the lignin, while the characteristics of the lignin showed prominent changes with the participation of the catalyst: the extraction rate increased from 71.65% to 98.13%, the purity was improved from 85.62% to 97.09%, and both the number average molecular weight and the weight average molecular weight also decreased significantly. Besides, the molecular distribution of the lignin achieved from the CC-LA-Fe-Si- $\text{V}_3$  reaction system was found to be more highly concentrated (Polydispersity index = 1.746). Results from 2D NMR HSQC analysis indicated that lignin fractions achieved from the CC-LA-Fe-Si- $\text{V}_3$  system showed distinct destruction involving  $\text{C}_2\text{-H}_2$  in guaiacyl units (G),  $\text{C}_5\text{-H}_5$  in guaiacyl units (G), and the  $\text{C}_\gamma\text{-H}_\gamma$  in  $\gamma$ -hydroxylated  $\beta\text{-O-4}'$  substructures, but little changes in the  $\text{C}_\gamma\text{-H}_\gamma$  in phenylcoumaran substructures.

**Keywords:** lignin extraction; magnetic catalyst; deep eutectic solvent; corncob



**Citation:** Yuan, M.; Wang, Z.; Liu, Y.; Yang, G. Fabrication of Magnetic Catalyst  $\text{Fe}_3\text{O}_4\text{-SiO}_2\text{-V}_3$  and Its Application on Lignin Extraction from Corncob in Deep Eutectic Solvent. *Polymers* **2021**, *13*, 1545. <https://doi.org/10.3390/polym13101545>

Academic Editor: Alejandro Sosnik

Received: 13 April 2021

Accepted: 7 May 2021

Published: 12 May 2021

**Publisher's Note:** MDPI stays neutral with regard to jurisdictional claims in published maps and institutional affiliations.



**Copyright:** © 2021 by the authors. Licensee MDPI, Basel, Switzerland. This article is an open access article distributed under the terms and conditions of the Creative Commons Attribution (CC BY) license (<https://creativecommons.org/licenses/by/4.0/>).

## 1. Introduction

As the second most abundant biopolymer in nature, lignin is the only non-petroleum resource that provides renewable aromatic compounds [1]. Annually, more than 50 million tons of lignin-based materials are produced, mainly by the pulp and paper industries [2]. However, less than 2% of them can be valorized and the vast majority of them are burned and used for energy recovery at the pulp mills [3]. Since the valorization of lignin highly affects the performance of biorefinery processes, it is imperative to develop various processes for lignin valorization. However, the extraction methods seriously restrain the subsequent bio-refinery processes. Lignins derived from traditional kraft pulping, sulfite cooking, and organosolv pulping usually exhibit unsatisfactory performance due to their low extraction rate, low purity, unevenly molecular weight distribution, poor reaction activity, and condensed structures [4]. The characteristics and extraction rate of lignin have significant influence on lignin valorization [5].

Deep eutectic solvents (DESs) are a new class of ionic liquids based on eutectic mixtures of hydrogen bond acceptor (HBA) and hydrogen bond donor (HBD). Compared with traditional ionic liquids, DESs have the advantages of low costs, biopolymer dissolution capability, biodegradability, nontoxicity, polarity, and recyclability, which make them appropriate media for biomaterials processing. In previous research, DESs exhibited perfect performance in the field of lignocellulosic biomass treatment [6]. They are reported to be beneficial to the processes of delignification, components dissolubility, conversion of lignocellulosic waste, and cellulose treatment (dissolution, modification, etc.) [7]. Among them,

CC/lactic acid, betaine/lactic acid, and some amino acid-based DESs (lactic acid/proline, malic acid/proline, malic acid/glycine) were found to have advantages in dissolving lignin and to exhibit tiny cellulose solubility. The lignin extraction rate of wheat straw is about 58% in the CC/oxalic acid dihydrate (1:1) system [6]. The lignin extraction efficiency of the ChCl/oxalic acid dihydrate system can reach 80% under the conditions of 110 °C and 9 h with the assistance of microwaves (800 W, 80 °C). The obtained lignin fraction (LF) possesses a low molecular weight (913 g·mol<sup>-1</sup>), low polydispersity (1.25), and high purity [8]. Abdulmalek and his co-workers reported that around 47% lignin and 87% hemicellulose were removed from oil palm trunk fibers in the ethylammonium chloride/ethylene glycol (molar ratio 1:2) system, and that the obtained pretreated fibers showed excellent enzymatic hydrolysis performance [9].

As new types of catalytic materials, heteropolyacids (HPAs) and polyoxometalates (POMs) have attracted people's attention due to their unique advantages of good acidity and redox properties [9–11]. In previous research, polyoxometalates were utilized as reagents or catalysts to control the extent of lignin oxidation during pulping or oxygen-based pulp bleaching processes [12–14]. However, some drawbacks which include low surface areas (1–5 m<sup>2</sup>·g<sup>-1</sup>), high solubility in polar solvents [15], and poor reusability [16] restrained their application. Considerable strategies were adopted to overcome these drawbacks. Among them, transition metals substitution was proven to effectively decrease their water solubility and enhance their reusability [17–21]. Immobilization of POMs on the supporters were also proven effective to enhance their performances, while different materials which include mesoporous silica, metal-organic frameworks (MOFs), metal oxides, and carbon materials were employed as supporters [22]. The modified POMs showed high reactivity and were successfully employed in the fields of electrochemistry, photochemistry, energy storage, and environmental protection [23].

In recent years, some researchers further explored the application of POMs in biorefinery processes. Xu et al. employed cesium substituted heterogeneous polyoxometalates as catalysts to improve birch lignin depolymerization in a mixture of CH<sub>3</sub>OH and H<sub>2</sub>O<sub>2</sub> (4:1, *v/v*), and found that the catalyst was easily separated from products and possessed perfect reusability [17]. Ru/POM nanocatalyst also displayed high activity and selectivity in oxidative depolymerization and could be recovered easily [18]. Keggin-type polyoxometalate-supported Au nanoparticles were conducted as catalysts to converse cellobiose into gluconic acid in the presence of O<sub>2</sub> when the highest cellobiose conversion and gluconic acid selectivity were ≥95% and 85%, respectively [19]. Zhang et al. proved that Mo-containing polyoxometalates were efficient for the conversion of cellulose into glycolic acid in water in O<sub>2</sub> when the glycolic acid yield was about 49% under optimal conditions [20]. Wölfel et al. reported that vanadium-substituted polyoxometalate could oxidize glucose to formic acid under 343–363 K and an O<sub>2</sub> pressure of 30 bar, while the yield of formic acid was about 50% [21].

Although DESs have been widely applied in the field of lignocellulosic biomass treatment, there are still many difficulties that need to be overcome. The processes usually need high temperatures and a long reaction time; the reusability of the catalysts still pose difficulties. The low extraction rate, low purity, and uneven molecular weight distribution of the obtained lignins significantly restrained the wide broad of this technology. To the best of our knowledge, there are still no reports that apply POMs as the catalyst to optimize the delignification process in DESs reaction systems [24,25]. In this research, Fe<sub>3</sub>O<sub>4</sub>-SiO<sub>2</sub>-V<sub>3</sub> was prepared by deposited H<sub>6</sub>PMo<sub>9</sub>V<sub>3</sub>O<sub>40</sub> on Fe<sub>3</sub>O<sub>4</sub>-SiO<sub>2</sub> and employed as an easy recovery magnetic catalyst. FTIR, SEM, and EDX mapping were carried out to prove the success of the preparations. Lignins obtained from the CC-LA system and CC-LA-Fe-Si-V<sub>3</sub> system were analyzed by Fourier-Transform Infrared (FT-IR), Gel Permeation Chromatography (GPC), and 2D-HSQC, respectively. Solid residues were also investigated by XRD. Reusability of the catalyst was also discussed.

## 2. Materials and Methods

### 2.1. Materials

We utilized corncob derived from Laiwu city, Shandong province. The raw corncob was washed with distilled water and ground into particles ranging from 40–60 mesh. Then, the powder was extracted by benzene-ethanol solution (benzene: ethanol = 2:1, volume ratio), dried at 60 °C for 6 h, and stored in a desiccator before application. The components of the corncob were analyzed according to the detection method of lignin and carbohydrate in biomass provided by NREL (National Renewable Energy Laboratory) [26]. Results indicated that it contains 40.12% cellulose, 32.74% xylan, 14.89% acid insoluble lignin, 1.96% acid soluble lignin, 3.67% ash, and 3.33% extraction.

### 2.2. Chemicals and Reagents

The chemicals and reagents used were: Choline chloride, sodium phosphate dibasic dodecahydrate, diethyl ether, iron chloride hexahydrate, ferrous sulfate, sulfuric acid (98%), hydrochloric acid (36%), ammonium hydroxide solution, and tetraethyl orthosilicate (Sinopharm Chemical Reagent Co. Ltd., Shanghai, China); sodium metavanadate, sodium molybdate dihydrate, dimethyl sulfoxide, anhydride, pyridine, and oleic acid (Shanghai Macklin Biochemical Technology Co., Ltd., Shanghai, China); Tetrahydrofuran, ethanol, and toluene (Tianjin Hengxing Chemical Reagent Co., Ltd., Tianjin, China); lactic acid, and potassium bromide (Tianjin Kemiou Chemical Reagents Co. Ltd., Tianjin, China).

### 2.3. Preparation of DES

Deep eutectic solvent was synthesized according to the method described in previous literature [27]. Choline chloride and lactic acid were vacuum dried at 80 °C for 5 h before use. The molar ratio between choline chloride and lactic acid was set as 1:10 according to the results of our previous research. The mixture was stirred in an oil bath at 60 °C for 2 h until a homogeneous clear liquid was formed.

### 2.4. Preparation of the Catalyst

The preparation of  $H_{3+x}PMo_{12-x}V_xO_{40}$  ( $x = 1-3$ ) was modified according to the method described in previous research [20,28]. Briefly, we put 50 mL  $NaVO_3$  ( $0.15 \text{ mol}\cdot\text{L}^{-1}$ ) and 50 mL  $Na_2HPO_4$  ( $0.025 \text{ mol}\cdot\text{L}^{-1}$ ) into a 500-mL beaker in order. Then, 3 mL sulfuric acid (98%,  $v/v$ ) and 100 mL  $Na_2MoO_4$  solution ( $1.0 \text{ mol}\cdot\text{L}^{-1}$ ) were added into the beaker in sequence. Next, 42 mL sulfuric acid (98%,  $v/v$ ) was added into the mixture slowly under vigorous stirring. The mixture was then extracted with ether to get red solids. We dissolved the red solids in 50 mL water, and put them in a vacuum dryer, while the solid product was placed in a dryer before use. Afterwards, 16.2 g  $FeCl_3\cdot 6H_2O$  and 8.34 g  $FeSO_4\cdot 7H_2O$  were dissolved in 125 mL distilled water, then we poured 185 mL boiling distilled water into the solution. Then, we added 33 mL ammonia into the mixture and stirred for 0.5 h. The precipitation was separated and washed with distilled water to obtain  $Fe_3O_4$ . Next, 8.0 g  $Fe_3O_4$  was dispersed in 400 mL water, while oleic acid was added in at the same time to increase the uniformity of the solution. We then added 3.04 mL TEOS and 8.28 mL ammonia into the mixture. Finally, the particles were separated by magnetic force and washed with distilled water.  $Fe_3O_4\text{-}SiO_2$  was obtained by drying at 48 °C overnight. We added 0.6 g  $Fe_3O_4\text{-}SiO_2$  particles, 12.0 mL distilled water, 6.0 mL TEOS, 8.4 mL ethanol, and 1.2 mL of 0.01 M  $HNO_3$  into a 50-mL beaker; the mixture reacted under 40 °C until sol was formed. A certain amount of  $H_6PMo_9V_3O_{40}$  was dissolved in 20.0 mL of ethanol and was slowly added into the sol. We kept stirring at 60 °C until a gel appeared;  $Fe_3O_4\text{-}SiO_2\text{-}V_3$  can be obtained by drying the gel at 100 °C for 10 h [29,30].

### 2.5. The Extraction Process of Lignin

Next, 2.0 g corncob powder was dispersed evenly into 60 g CC-LA (10:1). Then, a certain amount of the catalyst (0 and 0.06 g) was added into the reaction system and heated

to the required temperature (90–130 °C) by oil bath. The mixture was kept under a certain temperature for 9–15 h.

The mixture was filtered by G2. In addition, the solid residue was washed with anhydrous ethanol 3–5 times, then it was placed into an oven and dried under 90 °C until a constant mass was obtained ( $m_1$ ). The filtrate was treated by rotary evaporation to remove residual ethanol. Then, 2000 mL deionized water was added and fully stirred for 24 h; the precipitate was separated by centrifugation and washed with ethanol solution more than three times. The lignin powder ( $m_2$ ) was obtained by vacuum freeze-drying after centrifugation. Figure 1 exhibits the whole process.

$$X = \frac{m_1}{m_0} \times 100\% \quad (1)$$

$$Y = \frac{m_2}{m_0 \times w} \times 100\% \quad (2)$$

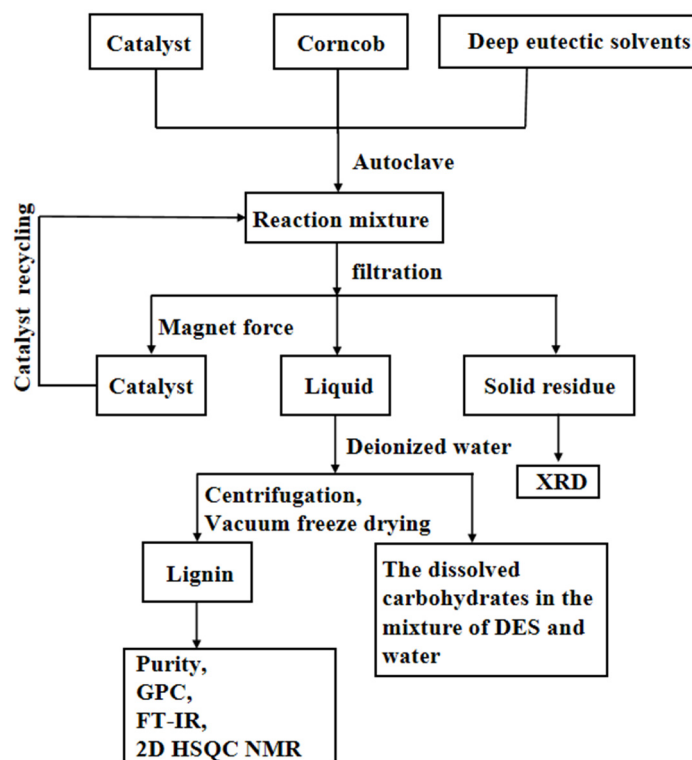


Figure 1. Flow diagram of the lignin extraction process.

X: percentage of solid residue quality, %;

Y: lignin extraction rate, %;

$m_0$ : quality of corncob, g;

$m_1$ : quality of solid residue, g.

$m_2$ : quality of lignin, g;

w: lignin content in corncob, %.

## 2.6. Samples Characterization and Calculation

### 2.6.1. Characterization of the Catalyst

The surface microstructure of  $\text{Fe}_3\text{O}_4\text{-SiO}_2$  and  $\text{Fe}_3\text{O}_4\text{-SiO}_2\text{-V}_3$  was observed by cold field emission scanning electron microscopy (SEM) Hitachi S4800. First, the double-sided conductive adhesive was glued to the copper base, so that the sample would be uniformly glued to the conductive adhesive. The sample was placed in the spraying room for gold spraying treatment, and then the sample was placed in the electron microscope observation

room, and the magnification of scanning electron microscope was adjusted to observe the surface morphology of the sample.

EDX allows the determination of the content and distribution of each element on the surface of a sample, depending on the wavelength of the characteristic X-rays of the different elements. The EDX was used to determine the content of each element in Fe<sub>3</sub>O<sub>4</sub>-SiO<sub>2</sub>-V<sub>3</sub> samples.

The diffraction patterns of untreated corncob and the solid residues after reaction were analyzed and determined by X-ray diffractometer (D8-Advance, Bruker, Germany). The scanning angle was set as 10–40°, 5°·min<sup>-1</sup>, the step size was 0.01°, the voltage was 40 kV, and the current was 40 mA.

### 2.6.2. Characterization and Calculation of the Corncob and the Products

IR spectra were recorded on a PerkinElmer “Spectrum BX” spectrometer in the 4000–400 cm<sup>-1</sup> region.

Lignin purity was carried out under following process: at first, 0.3 g of lignin and 3 mL of 72% concentrated sulfuric acid were added to a pressure resistant flask and reacted at 30 °C for 1 h. Then, 84 mL of deionized water was added to the flask and the reaction was carried out at 121 °C for 6 min. Next, lignin was filtered through an inorganic 0.22 µm filter membrane and detected by ion chromatography. The ratio of the sum of acid soluble lignin and acid insoluble lignin to the mass of lignin is the purity of the lignin.

The molecular weight of lignin was determined by gel permeation chromatograph (Waters e2695 Alliance HPLC, MA, USA). A total of 10 mg acetylated lignin was completely dissolved in 10 mL tetrahydrofuran solvent. The sample size was 10 µL, and the flow rate was 40 °C and 0.6 mL·min<sup>-1</sup>, respectively. The chromatographic column was Plgel Mixed-E (7.5 mm × 300 mm, 3 µm). The standard curve was determined by using the polystyrene standard with a different relative molecular weight.

The 2D-HSQC NMR spectra of the achieved lignin were conducted on AVANCE II 400 using 0.75 mL of DMSO d<sub>6</sub> mixed with 0.1 mL pyridine d<sub>5</sub> at room temperature.

The crystallinity index was calculated by the peak height method [31].

$$\text{CrI} = \frac{I_{002} - I_{\text{am}}}{I_{002}} \times 100\% \quad (3)$$

$I_{002}$  is the intensity of 002 lattice diffraction ( $2\theta = 22.7^\circ$ );

$I_{\text{am}}$  is the intensity of amorphous section ( $2\theta = 16.5^\circ$ ).

## 3. Results and Discussion

### 3.1. Characteristics of the Catalyst

The SEM images of Fe<sub>3</sub>O<sub>4</sub>-SiO<sub>2</sub> and Fe<sub>3</sub>O<sub>4</sub>-SiO<sub>2</sub>-V<sub>3</sub> are shown in Figure 2a–d. The particle sizes of the products were measured by ImageJ 1.8.0. Results indicate the statistical particle size of Fe<sub>3</sub>O<sub>4</sub>-SiO<sub>2</sub> is in the range of 35–50 nm. The statistical particle size of Fe<sub>3</sub>O<sub>4</sub>-SiO<sub>2</sub>-V<sub>3</sub> is in the range of 60–80 nm. The precipitation of V<sub>3</sub> on the surface of Fe<sub>3</sub>O<sub>4</sub>-SiO<sub>2</sub> led to the increase of the particle size.

Figure 2e showed the EDX of Mo, V, and P distribution in Fe<sub>3</sub>O<sub>4</sub>-SiO<sub>2</sub>-V<sub>3</sub>. The appearance of P, Mo, and V in the EDX mapping of Fe<sub>3</sub>O<sub>4</sub>-SiO<sub>2</sub>-V<sub>3</sub> proved that V<sub>3</sub> loaded onto Fe<sub>3</sub>O<sub>4</sub>-SiO<sub>2</sub> successfully. Furthermore, the results of Figure 2f–h also showed that V, Mo, and P were uniformly dispersed on the supporter.

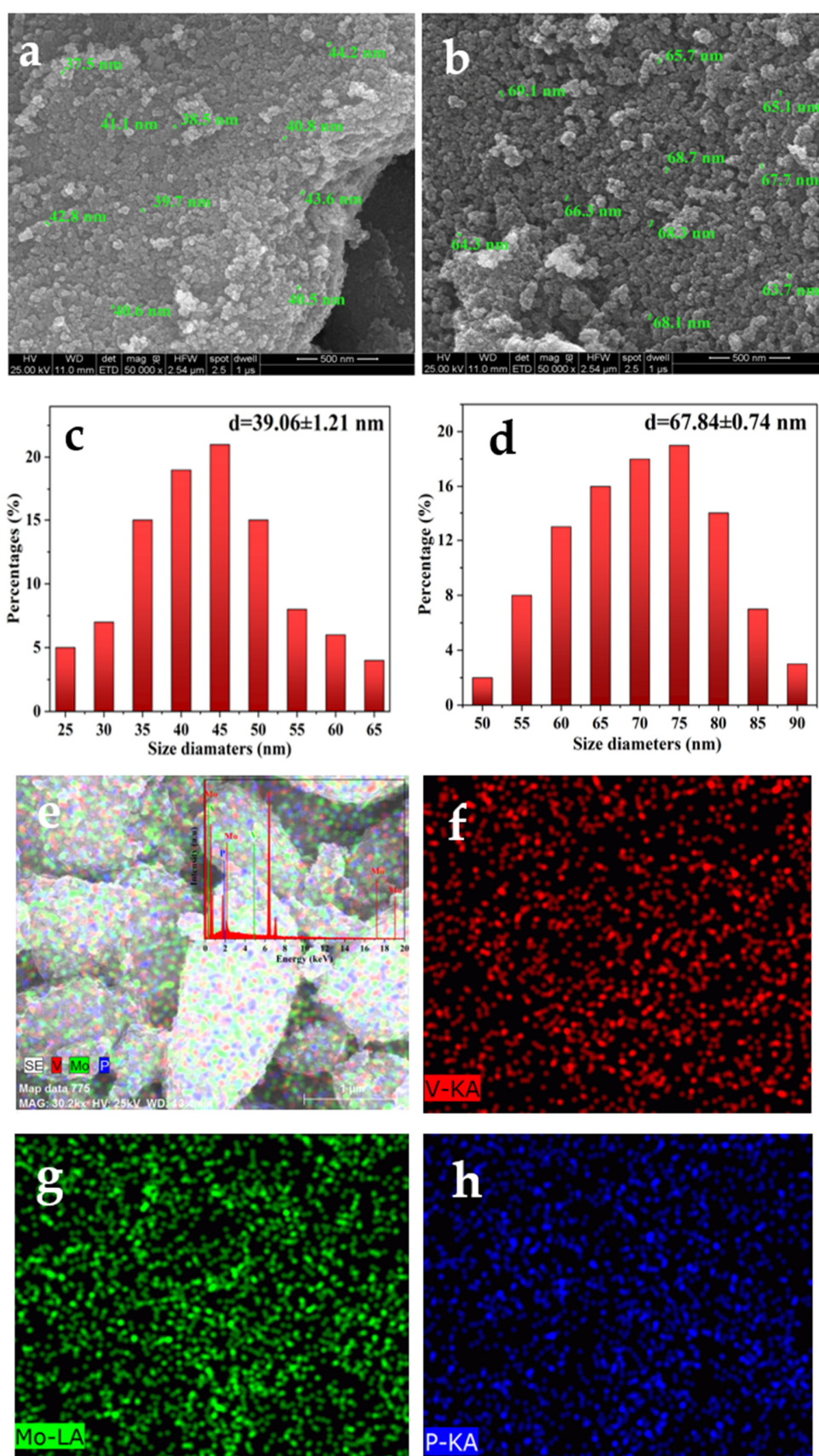


**Figure 2.** (a) SEM images of  $\text{Fe}_3\text{O}_4\text{-SiO}_2$ ; (b) SEM images of  $\text{Fe}_3\text{O}_4\text{-SiO}_2\text{-V}_3$ ; (c) size distribution of  $\text{Fe}_3\text{O}_4\text{-SiO}_2$ ; (d) size distribution of  $\text{Fe}_3\text{O}_4\text{-SiO}_2\text{-V}_3$ ; (e) EDX mapping of  $\text{Fe}_3\text{O}_4\text{-SiO}_2\text{-V}_3$ ; (f) elemental mapping of V; (g) elemental mapping of Mo; (h) elemental mapping of P.

### 3.2. Calculation of Crystallinity of Solid Residue

XRD spectra of untreated corncob and the solid residues after reaction were shown in Figure 3. The peak appeared  $2\theta = 16.5^\circ$  and  $22.7^\circ$  indicated the cellulose structure of corncob should belong to type I.

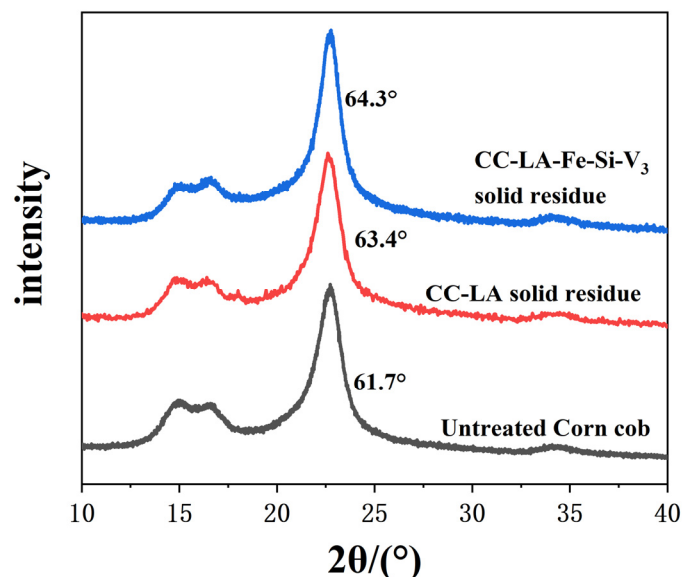


**Figure 3.** X-ray diffraction analysis spectra of various cellulose samples.

The crystallinity of untreated corncob was 61.7%, the crystallinity of CC-LA solid residue and CC-LA-Fe-Si-V<sub>3</sub> solid residue was 63.4° and 64.3°, respectively. The crystallinity of the two solid residues treated by deep eutectic solvent and magnetic the catalyst was higher than that of the untreated corncob. However, the crystallinity of CC-LA-Fe-Si-V<sub>3</sub> solid residue was higher than that of CC-LA solid residue. This might be attributed to the magnetic catalyst that destroyed the link between lignin and hemicellulose and removed lignin. The relative content of cellulose content of cellulose components led to the increase in the crystallinity of CC-LA-Fe-Si-V<sub>3</sub> solid residue.

### 3.3. Characterization of Lignin

Table 1 shows the purity changes of CC-LA lignin and CC-LA-Fe-Si-V<sub>3</sub> lignin at different temperatures. When the reaction temperature increased from 90 °C to 120 °C, there were little fluctuate occurred for both reaction systems. The variation range of purity for CC-LA lignin was 85.6%–86.8%. Meanwhile, it was 97.1–98.3% for CC-LA-Fe-Si-V<sub>3</sub> lignin. When the temperature increased to 130 °C, the lignin purities for both reaction systems decreased. The purity of CC-LA-Fe-Si-V<sub>3</sub> lignin was significantly higher than that of CC-LA lignin. This proved that the application of magnetic the catalyst was beneficial for improving the purity of lignin.

**Table 1.** Purities of CC-LA lignin and CC-LA-Fe-Si-V<sub>3</sub> lignin.

	90 °C	100 °C	110 °C	120 °C	130 °C
CC-LA lignin (%)	86.82	86.5	86.1	85.62	82.35
CC-LA-Fe-Si-V <sub>3</sub> lignin (%)	98.25	97.75	97.6	97.09	95.34

Table 2 displayed the variation of the heavy average molecular weight ( $M_w$ ) and number average molecular weight ( $M_n$ ) of CC-LA lignin and CC-LA-Fe-Si-V<sub>3</sub> lignin with the reaction temperature. Results showed that the  $M_w$  and  $M_n$  of both reaction systems had a declining tendency with the increase of the reaction temperature. The  $M_w$

of CC-LA lignin decreased from  $1752 \text{ g}\cdot\text{mol}^{-1}$  to  $1366 \text{ g}\cdot\text{mol}^{-1}$  and the  $M_n$  decreased from  $900 \text{ g}\cdot\text{mol}^{-1}$  to  $731 \text{ g}\cdot\text{mol}^{-1}$ . The  $M_w$  of CC-LA-Fe-Si-V<sub>3</sub> lignin decreased from  $1482 \text{ g}\cdot\text{mol}^{-1}$  to  $1142 \text{ g}\cdot\text{mol}^{-1}$  and the  $M_n$  decreased from  $773 \text{ g}\cdot\text{mol}^{-1}$  to  $654 \text{ g}\cdot\text{mol}^{-1}$ . This could be attributed to the fact that the increase in reaction temperature facilitated the breaking of the  $\beta$ -O-4 bond [32]. The  $M_w$  and  $M_n$  of CC-LA-Fe-Si-V<sub>3</sub> lignin were lower than those of CC-LA lignin, regardless of the change in reaction temperature. This might have been because of the CC-LA-Fe-Si-V<sub>3</sub> reaction system facilitating the cleavage of the lignin-carbohydrate complex (LCC) [33].

**Table 2.** Average molecular weights and polydispersity indexes (PDI) of different lignins.

		90 °C	100 °C	110 °C	120 °C	130 °C
CC-LA lignin	$M_w$ ( $\text{g}\cdot\text{mol}^{-1}$ )	1752	1521	1461	1384	1366
	$M_n$ ( $\text{g}\cdot\text{mol}^{-1}$ )	909	795	776	740	731
	PDI	1.93	1.91	1.88	1.87	1.87
CC-LA-Fe-Si-V <sub>3</sub> lignin	$M_w$ ( $\text{g}\cdot\text{mol}^{-1}$ )	1482	1451	1371	1336	1142
	$M_n$ ( $\text{g}\cdot\text{mol}^{-1}$ )	773	772	751	738	654
	PDI	1.92	1.88	1.83	1.81	1.75

The polydispersity index (PDI) of lignin was calculated by the weight average molecular weight and number average molecular weight ratio ( $M_w/M_n$ ) of lignin. The polydispersity index of CC-LA lignin was in the range of 1.93–1.87. The polydispersity index of CC-LA-Fe-Si-V<sub>3</sub> lignin ranged from 1.92 to 1.75. Compared with CC-LA lignin, CC-LA-Fe-Si-V<sub>3</sub> lignin had a lower polydispersity index, indicating that the molecular distribution of CC-LA-Fe-Si-V<sub>3</sub> lignin was relatively narrow.

Figure 4 shows the FT-IR spectra results of the lignins obtained from both reaction systems. CC-LA-Fe-Si-V<sub>3</sub> lignin presented similar absorbance bands with those of CC-LA lignin. Peaks that appeared at  $3420 \text{ cm}^{-1}$  and  $2930 \text{ cm}^{-1}$  corresponded to the stretching mode of O-H and the aliphatic C-H stretching related to the methoxy group, respectively [34]. The bands presented at  $1715 \text{ cm}^{-1}$  and  $1510 \text{ cm}^{-1}$  were associated with C=O stretching in unconjugated carbonyl and carboxyl groups and skeletal and stretching vibrations of benzene rings. The absorption at  $1450 \text{ cm}^{-1}$  was associated with aromatic ring vibration. The absorption at  $1375 \text{ cm}^{-1}$  was associated with C-C stretching of the S unit.

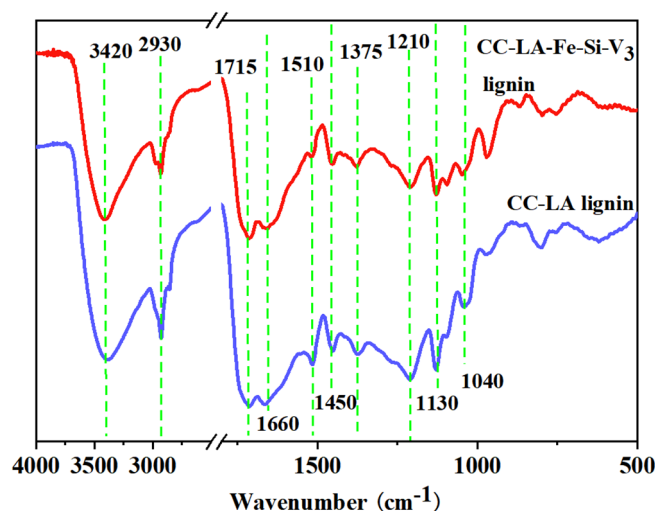


**Figure 4.** FT-IR analysis of CC-LA lignin and CC-LA-Fe-Si-V<sub>3</sub> lignin.

In addition, the characteristic signal of the skeletal and stretching vibrations of benzene rings and lignin structures occurred at  $1510 \text{ cm}^{-1}$  [35]. Moreover, the signal of C=O stretching vibration of the guaiacyl (G) unit occurred at  $1210 \text{ cm}^{-1}$  [36]. It was noticed that the signal was clearly more distinct in CC-LA lignin than in CC-LA-Fe-Si-V<sub>3</sub> lignin, which



indicated that the addition of  $\text{Fe}_3\text{O}_4\text{-SiO}_2\text{-V}_3$  led more aromatic rings to be decomposed and to the destruction of more guaiacyl (G) units. In addition, the peaks exhibited at  $1130\text{ cm}^{-1}$  and  $1040\text{ cm}^{-1}$  should belong to the characteristic signals of C-H stretching vibration of syringyl units and C-H bending vibration of guaiacyl units in a lignin structure [37].

To elucidate the characteristics of the CC-LA-Fe-Si-V<sub>3</sub> lignin more clearly, the structure and chemical composition of lignin as extracted by 2D-HSQC NMR were analyzed. The 2D-HSQC spectra of CC-LA lignin and CC-LA-Fe-Si-V<sub>3</sub> lignin are shown in Figure 5. In the 2D-HSQC NMR spectra of the ( $\delta\text{C}/\delta\text{H}$ , 45–90 ppm/2.0–6.0 ppm) region, there mainly is a methoxy group with a  $\beta\text{-O-4}$  structure (A) and  $\beta\text{-O-4}$  acetylated structure (A') in CC-LA lignin. The  $\alpha$  position of  $\beta\text{-O-4}$  linkages appeared at ( $\delta\text{C}/\delta\text{H}$ , 68.41/5.02 ppm) and ( $\delta\text{C}/\delta\text{H}$ , 72.96/4.72 ppm). The  $\beta$  position of  $\beta\text{-O-4'}$  linkages was exhibited at ( $\delta\text{C}/\delta\text{H}$ , 80.79/4.56 ppm) and ( $\delta\text{C}/\delta\text{H}$ , 84.21/4.25 ppm) [38,39]. The correlation of  $\text{C}_\gamma\text{-H}_\gamma$  in the  $\gamma$ -acylated lignin unit (A' $_\gamma$ ) was observed at ( $\delta\text{C}/\delta\text{H}$ , 65.67/4.18 ppm). In addition, the spectra of CC-LA lignin components also showed a p-hydroxycinnamyl alcohol end group, phenylcoumaran substructures (B $_\gamma$ ), and  $\beta\text{-}\beta'$  resinol substructures (C $_\beta$ ).

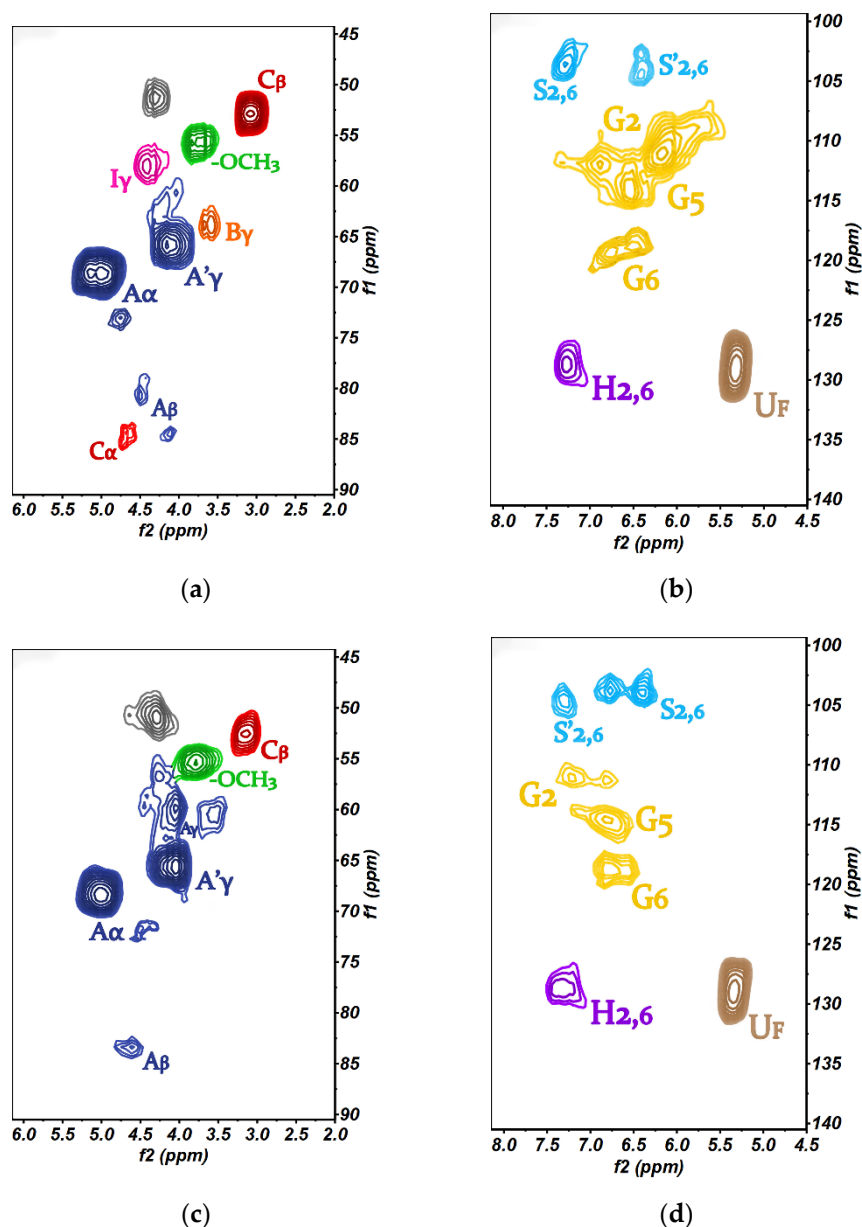
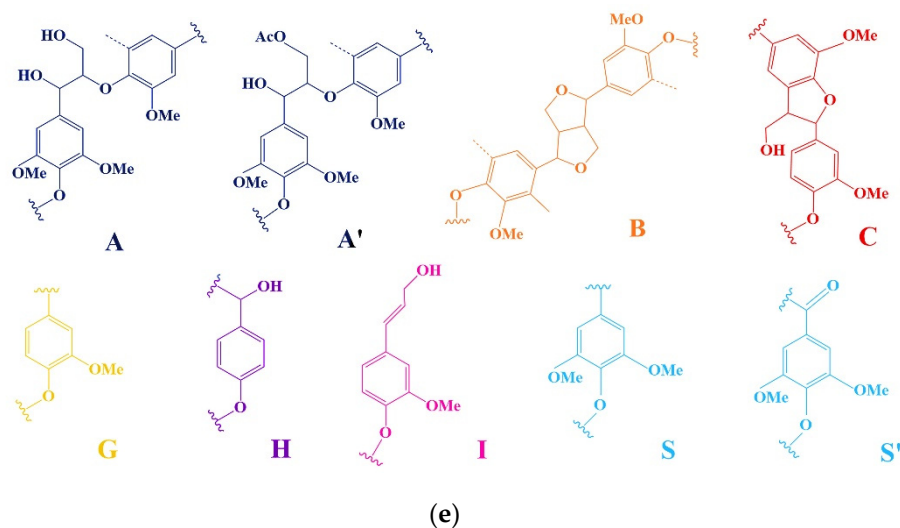


Figure 5. Cont.



**Figure 5.** (a,c) The 2D-HSQC NMR spectra of CC-LA Lignin; (b,d) The 2D-HSQC NMR spectra of CC-LA-Fe-Si-V<sub>3</sub> lignin; (e) The structure of various functional groups in 2D-HSQC NMR spectra.

In the 2D-HSQC NMR spectra of CC-LA-Fe-Si-V<sub>3</sub> lignin, the  $\alpha$  position of  $\beta$ -O-4 linkages was exhibited at ( $\delta\text{C}/\delta\text{H}$ , 68.31/5.02 ppm) and ( $\delta\text{C}/\delta\text{H}$ , 72.21/4.52 ppm). The  $\beta$  position of  $\beta$ -O-4' linkages appeared at ( $\delta\text{C}/\delta\text{H}$ , 83.56/4.61 ppm). The correlation of  $\text{C}_\gamma$ - $\text{H}_\gamma$  in a  $\gamma$ -acylated lignin unit ( $\text{A}'\gamma$ ) was observed at ( $\delta\text{C}/\delta\text{H}$ , 65.64/4.05 ppm). In addition, resinol substructures appeared at ( $\delta\text{C}/\delta\text{H}$ , 52.93/3.14 ppm) and a p-hydroxycinnamyl alcohol end group (I) was observed at ( $\delta\text{C}/\delta\text{H}$ , 57.03/4.27 ppm). CC-LA lignin contains the  $\text{C}_\gamma$ - $\text{H}_\gamma$  phenylcoumaran substructures ( $\delta\text{C}/\delta\text{H}$  63.71/3.61). CC-LA-Fe-Si-V<sub>3</sub> lignin has the  $\text{C}_\gamma$ - $\text{H}_\gamma$  in  $\gamma$ -hydroxylated  $\beta$ -O-4' substructures ( $\delta\text{C}/\delta\text{H}$ , 60.66/3.58 ppm) [40]. This is the main difference between the CC-LA lignin and CC-LA-Fe-Si-V<sub>3</sub> lignin.

In the 2D-HSQC NMR spectra of the ( $\delta\text{C}/\delta\text{H}$ , 100~140 ppm/4.5~8.0 ppm) region, there are S and G units of lignin. In the 2D-HSQC NMR spectra of CC-LA lignin, a  $\text{C}_{2,6}$ - $\text{H}_{2,6}$  signal of S units was found at ( $\delta\text{C}/\delta\text{H}$ , 104.63/6.41 ppm) and ( $\delta\text{C}/\delta\text{H}$ , 104.75/7.45 ppm). In the 2D-HSQC NMR spectra of CC-LA-Fe-Si-V<sub>3</sub> lignin, a  $\text{C}_{2,6}$ - $\text{H}_{2,6}$  signal of S units was observed at ( $\delta\text{C}/\delta\text{H}$ , 104.19/6.59 ppm) and ( $\delta\text{C}/\delta\text{H}$ , 105.31/7.21 ppm) [41,42]. In the 2D-HSQC NMR spectra of CC-LA lignin,  $\text{C}_2$ - $\text{H}_2$ ,  $\text{C}_5$ - $\text{H}_5$ , and  $\text{C}_6$ - $\text{H}_6$  of G unit were observed at ( $\delta\text{C}/\delta\text{H}$ , 111.78/7.03 ppm), ( $\delta\text{C}/\delta\text{H}$ , 115.47/6.68 ppm), and ( $\delta\text{C}/\delta\text{H}$ , 119.61/6.73 ppm), respectively. In the 2D-HSQC NMR spectra of CC-LA-Fe-Si-V<sub>3</sub> lignin,  $\text{C}_2$ - $\text{H}_2$ ,  $\text{C}_5$ - $\text{H}_5$ , and  $\text{C}_6$ - $\text{H}_6$  of G unit were observed at ( $\delta\text{C}/\delta\text{H}$ , 111.89/7.34 ppm), ( $\delta\text{C}/\delta\text{H}$ , 115.21/6.43 ppm), and ( $\delta\text{C}/\delta\text{H}$ , 119.32/6.65 ppm), respectively [43]. In addition, strong linoleic acid signals were found in the spectrum.

CC-LA lignin and CC-LA-Fe-Si-V<sub>3</sub> lignin samples possess an intact structure. More  $\text{C}_2$ - $\text{H}_2$  and  $\text{C}_5$ - $\text{H}_5$  in G units of CC-LA-Fe-Si-V<sub>3</sub> lignin were destroyed than CC-LA lignin. This further proves the results of FT-IR spectra.  $\text{Fe}_3\text{O}_4$ - $\text{SiO}_2$ -V<sub>3</sub> has both destructive and protective functions on the different structures of lignin. In the 2D-HSQC NMR spectra of CC-LA-Fe-Si-V<sub>3</sub> lignin,  $\text{C}_\gamma$ - $\text{H}_\gamma$  in phenylcoumaran substructures were protected. Additionally,  $\text{C}_\gamma$ - $\text{H}_\gamma$  in  $\gamma$ -hydroxylated  $\beta$ -O-4' substructures was destroyed.

### 3.4. Possible Mechanism of the Catalysis Process

The mechanism of the delignification process catalyzed by POMs mainly affects their swift reversible multi-electron redox transformation property and variable acid-base and redox properties, which result in high conversion and selectivity through benzylic alcohol oxidation [11,44]. Figure 6 indicates the might mechanism of the delignification process of the CC-LA-PMoV<sub>3</sub> reaction system.

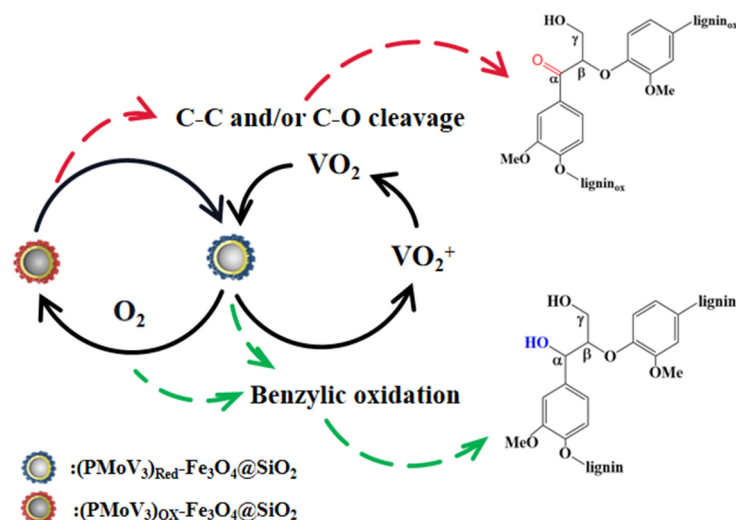
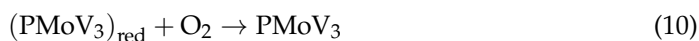
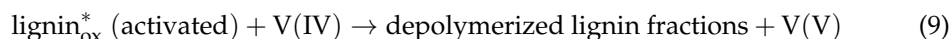
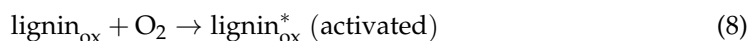
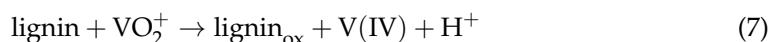
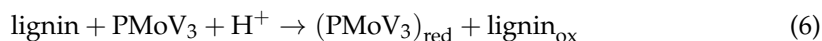


**Figure 6.** Possible mechanism of the delignification process.

In acidic solutions,  $\text{PMoV}_3$  could disproportionate and provide species with a number of vanadium atoms which are different from the original molecular structure [45]:



The anodic potentials of lignin structural units which bear phenolic hydroxyl groups are usually in the range +0.40 to +0.60 V [46]. Meanwhile, the reduction potentials of  $\text{PMoV}_n$  ( $n = 1-3$ ) are in the range +0.68 to +0.778 V, and the oxidation potential of  $\text{VO}_2^+$  is about 0.87 V. Thus, the redox potential of the reaction system is enough to satisfy the thermodynamic conditions for the catalytic oxidation of the lignin in corncob. During the delignification process, the  $\text{C}_\alpha$  structure which possesses a hydroxy unit can be activated by the catalysts and selectively oxidized to lignin<sub>ox</sub>, then it could be further oxidized by  $\text{VO}_2^+$  and promote the cleavage of the benzylic units [21]. Secondly, the reduced  $\text{PMoV}_3$  and  $\text{VO}_2$  could be turned to oxidized  $\text{PMoV}_3$  and  $\text{VO}_2^+$  with the assistance of  $\text{O}_2$ . During this process, the cleavage of  $\beta$ -O-4 ether and  $\text{C}_\alpha$ - $\text{C}_\beta$  linkages would occur under the assistance of acidic conditions. A related mechanism could be described as Equations (6)–(10).



### 3.5. Reusability of the Magnetic Catalyst

After the reaction was separated and recovered, the supported the catalyst and the mixed solution of ethanol and water (ethanol: water = 1:9) were used for centrifugal washing and drying. The lignin extraction rates from the first to the sixth reaction of  $\text{Fe}_3\text{O}_4\text{-SiO}_2\text{-V}_3$  were 98.1%, 96.4%, 94.9%, 93.6%, 93.1%, and 92.8%, respectively. After six reactions, the supported catalyst still had high activity, and the extraction rate of lignin decreased by only 5.3%. By comparing the structure of  $\text{Fe}_3\text{O}_4\text{-SiO}_2\text{-V}_3$  before and after the reaction, it was found that the magnetic catalyst  $\text{Fe}_3\text{O}_4\text{-SiO}_2\text{-V}_3$  had no significant change after repeated use, showing high stability.

#### 4. Conclusions

Both the CC-LA reaction system and the CC-LA-Fe-Si-V<sub>3</sub> reaction system were used to selectively separate lignin from corncob. The CC-LA-Fe-Si-V<sub>3</sub> reaction system has more advantages than the CC-LA reaction system. The extraction rate of lignin increased from 71.65% to 98.13%, while the purity of lignin increased from 85.62% to 97.09%. The CC-LA-Fe-Si-V<sub>3</sub> reaction system has both destructive and protective functions affecting the different structures of lignin. The CC-LA-Fe-Si-V<sub>3</sub> reaction system proposed in the present work could improve the extraction of lignin. CC-LA lignin and CC-LA-Fe-Si-V<sub>3</sub> lignin samples possess an intact structure. The aromatic rings and guaiacol units in CC-LA-Fe-Si-V<sub>3</sub> lignin were clearly destroyed. C<sub>γ</sub>-H<sub>γ</sub> in phenylcoumaran substructures in CC-LA-Fe-Si-V<sub>3</sub> lignin was protected, and C<sub>γ</sub>-H<sub>γ</sub> in γ-hydroxylated β-O-4' substructures was destroyed. Compared to CC-LA lignin, CC-LA-Fe-Si-V<sub>3</sub> lignin has a higher purity, lower molecular weight, and more concentrated distribution. CC-LA-Fe-Si-V<sub>3</sub> lignin showed more potential application values in chemical industries.

**Author Contributions:** Z.W. and M.Y. conceived and designed the experiments; M.Y. and Z.W. performed the experiments; Z.W., M.Y., and Y.L. analyzed the data; Z.W. and G.Y. contributed reagents/materials/analysis tools; Z.W. and M.Y. wrote the study; Y.L. and G.Y. reviewed the manuscript and made comments. All authors have read and agreed to the published version of the manuscript.

**Funding:** National Natural Science Foundation of China (31800219).

**Institutional Review Board Statement:** Not applicable.

**Informed Consent Statement:** Not applicable.

**Data Availability Statement:** Not applicable.

**Acknowledgments:** The authors are grateful to be supported in part by the National Key Research and Development Program (20190YFC1905904) and the Taishan Scholars Program Pilot Project for Integrating Science, Education, and Industry (2020KJC-ZD14).

**Conflicts of Interest:** The authors declare no conflict of interest.

#### References

1. Feofilova, E.P.; Mysyakina, I.S. Lignin: Chemical structure, biodegradation, and practical application (a review). *Appl. Biochem. Microbiol.* **2016**, *52*, 573–581. [[CrossRef](#)]
2. Norgren, M.; Edlund, H. Lignin: Recent advances and emerging applications. *Curr. Opin. Colloid Interface Sci.* **2014**, *19*, 409–416. [[CrossRef](#)]
3. Wang, H.; Pu, Y.; Ragauskas, A.; Yang, B. From Lignin to Valuable Products-Strategies, Challenges, and Prospects. *Bioresour. Technol.* **2018**, *271*, 449–461. [[CrossRef](#)] [[PubMed](#)]
4. Xu, C.; Arancon, R.A.D.; Labidi, J.; Luque, R. Lignin depolymerisation strategies: Towards valuable chemicals and fuels. *Chem. Soc. Rev.* **2014**, *43*, 7485–7500. [[CrossRef](#)] [[PubMed](#)]
5. Sathitsuksanoh, N.; Holtman, K.M.; Yelle, D.J.; Morgan, T.; Stavila, V.; Pelton, J.; Blanch, H.; Simmons, B.A.; George, A. Lignin fate and characterization during ionic liquid biomass pretreatment for renewable chemicals and fuels production. *Green Chem.* **2014**, *16*, 1236–1247. [[CrossRef](#)]
6. Francisco, M.; Bruinhorst, A.; Kroon, M.C. New natural and renewable low transition temperature mixtures (LTTMs): Screening as solvents for lignocellulosic biomass processing. *Green Chem.* **2012**, *14*, 2153–2157. [[CrossRef](#)]
7. Magdalena, Z.; Katarzyna, W.; Tadeusz, S. Deep eutectic solvents for polysaccharides processing. A review. *Carbohydr. Polym.* **2018**, *200*, 361–380. [[CrossRef](#)]
8. Liu, Y.; Chen, W.; Xia, Q.; Guo, B.; Wang, Q.; Liu, S.; Liu, Y.; Li, J.; Yu, H. Efficient Cleavage of Lignin-Carbohydrate Complexes and Ultrafast Extraction of Lignin Oligomers from Wood Biomass by Microwave-Assisted Treatment with Deep Eutectic Solvent. *ChemSusChem* **2017**, *10*, 1692–1700. [[CrossRef](#)]
9. Abdulmalek, E.; Zulkefli, S.; Rahman, M.B.A. Deep eutectic solvent as a media in swelling and dissolution of oil palm trunk. *Malays. J. Anal. Sci.* **2017**, *21*, 20–26. [[CrossRef](#)]
10. Zhang, C.W.; Xia, S.Q.; Ma, P.S. Facile pretreatment of lignocellulosic biomass using deep eutectic solvents. *Bioresour. Technol.* **2016**, 1–5. [[CrossRef](#)]
11. Procentese, A.; Johnson, E.; Orr, V.; Campanile, A.G.; Wood, J.A.; Marzocchella, A.; Rehmann, L. Deep eutectic solvent pretreatment and subsequent saccharification of corncob. *Bioresour. Technol.* **2015**, 31–36. [[CrossRef](#)]

12. Garcia Gonzalez, M.N.; Levi, M.; Turri, S.; Griffini, G. Lignin nanoparticles by ultrasonication and their incorporation in waterborne polymer nanocomposites. *J. Appl. Polym. Sci.* **2017**, *134*. [[CrossRef](#)]
13. An, Y.X.; Zong, M.H.; Wu, H.; Li, N. Pretreatment of lignocellulosic biomass with renewable cholinium ionic liquids: Biomass fractionation, enzymatic digestion and ionic liquid reuse. *Bioresour. Technol.* **2015**, *192*, 165–171. [[CrossRef](#)]
14. Jeon, Y.M.; Kim, J.; Whang, D.; Kim, K. Molecular Container Assembly Capable of Controlling Binding and Release of Its Guest Molecules: Reversible Encapsulation of Organic Molecules in Sodium Ion Complexed Cucurbituril. *J. Am. Chem. Soc.* **1996**, *118*, 9790–9791. [[CrossRef](#)]
15. Weinstock, I.A.; Atalla, R.H.; Reiner, R.S. A new environmentally benign technology for transforming wood pulp into paper. Engineering polyoxometalates as catalysts for multiple processes. *J. Mol. Catal. A Chem.* **1997**, *116*, 59–84. [[CrossRef](#)]
16. Evtuguin, D.V.; Neto, C.P.; Rocha, J. Oxidative delignification in the presence of molybdovanadophosphate heteropolyanions: Mechanism and kinetic studies. *Appl. Catal. A Gen.* **1998**, *167*, 123–139. [[CrossRef](#)]
17. Evtuguin, D.V.; Daniel, A.I.D.; Silvestre, A.J.D.; Amado, F.M.L.; Neto, C.P.; Mol, J. Lignin aerobic oxidation promoted by molybdovanadophosphate polyanion  $[\text{PMo}_7\text{V}_5\text{O}_{40}]^{8-}$ . Study on the oxidative cleavage of  $\beta$ -O-4 aryl ether structures using model compounds. *J. Mol. Catal. A Chem.* **2000**, 154–217. [[CrossRef](#)]
18. Guo, T.; Qiu, M.; Qi, X. Selective conversion of biomass-derived levulinic acid to ethyl levulinate catalyzed by metal organic framework (MOF)-supported polyoxometalates. *Appl. Catal. A Gen.* **2019**, *572*, 168–175. [[CrossRef](#)]
19. Benadji, S.; Eloy, P.; Leonard, A.; Su, B.L.; Rabia, C.; Gaigneaux, E.M. Characterization of  $\text{H}_{3+x}\text{PMo}_{12-x}\text{V}_x\text{O}_{40}$  heteropolyacids supported on HMS mesoporous molecular sieve and their catalytic performance in propene oxidation. *Micropor. Mesopor. Mat.* **2012**, *154*, 153–163. [[CrossRef](#)]
20. Dupont, P.; Védrine, J.C.; Paumard, E.; Hecquet, G.; Lefebvre, F. Heteropolyacids supported on activated carbon as catalysts for the esterification of acrylic acid by butanol. *Appl. Catal. A Gen.* **1995**, *129*, 217–227. [[CrossRef](#)]
21. Xu, W.; Li, X.; Shi, J. Catalytic depolymerization of lignin over cesium exchanged and transition-metal substituted heterogeneous polyoxometalates. *Int. J. Biol. Macromol.* **2019**, *135*, 171–179. [[CrossRef](#)]
22. Muñoz, J.; Cuentas-Gallegos, A.K.; Robles, M.; Valdéz, M. Bond formation, electronic structure, and energy storage properties on polyoxometalate/carbon nanocomposites. *Theor. Chem. Acc.* **2016**, *135*, 92. [[CrossRef](#)]
23. An, D.; Ye, A.; Deng, W. Selective Conversion of Cellobiose and Cellulose into Gluconic Acid in Water in the Presence of Oxygen, Catalyzed by Polyoxometalate-Supported Gold Nanoparticles. *Chemistry* **2012**, *18*, 2938–2947. [[CrossRef](#)] [[PubMed](#)]
24. Zhang, J.; Liu, X.; Sun, M. Direct Conversion of Cellulose to Glycolic Acid with a Phosphomolybdic Acid Catalyst in a Water Medium. *ACS Catal.* **2012**, *2*, 1698–1702. [[CrossRef](#)]
25. Wölfel, R.; Taccardi, N.; Bösmann, A.; Wasserscheid, P. Selective catalytic conversion of biobased carbohydrates to formic acid using molecular oxygen. *Green Chem.* **2011**, *13*, 2759–2763. [[CrossRef](#)]
26. Dizaji, A.K.; Mortaheb, H.R.; Mokhtarani, B. Preparation of supported catalyst by adsorption of polyoxometalate on graphene oxide/reduced graphene oxide. *Mater. Chem. Phys.* **2017**, *199*, 424–434. [[CrossRef](#)]
27. Baguc, I.B.; Saglam, S.; Ertas, I.E.; Keles, M.N.; Celebi, M.; Kaya, M.; Zahmakiran, M. Keggin Type-Polyoxometalate Decorated Ruthenium Nanoparticles: Highly Active and Selective Nanocatalyst for the Oxidation of Veratryl Alcohol as a Lignin Model Compound. *Chemistryselect* **2017**, *2*, 2487–2494. [[CrossRef](#)]
28. Tsigdinos, G.A. Preparation and Characterization of 12-Molybdophosphoric and 12-Molybdosilicic Acids and Their Metal Salts. *Chem. Inf.* **1974**, *13*, 267–274. [[CrossRef](#)]
29. Deng, Y.; Qi, D.; Deng, C.; Zhang, X.; Zhao, D. Superparamagnetic High-Magnetization Microspheres with an  $\text{Fe}_3\text{O}_4/\text{SiO}_2$  Core and Perpendicularly Aligned Mesoporous  $\text{SiO}_2$  Shell for Removal of Microcystins. *J. Am. Chem. Soc.* **2008**, *130*, 28. [[CrossRef](#)]
30. Hou, Y.; Ma, J.; Wang, T.; Fu, Q. Phosphotungstic acid supported on magnetic core-shell nanoparticles with high photocatalytic activity. *Mater. Sci. Semicond. Process.* **2015**, *39*, 229–234. [[CrossRef](#)]
31. Segal, L. An Empirical Method for Estimating the Degree of Crystallinity of Native Cellulose Using the X-Ray Diffractometer. *Text. Res. J.* **1959**, *29*, 786–794. [[CrossRef](#)]
32. Sun, S.N.; Li, M.F.; Yuan, T.Q.; Xu, F.; Sun, R.C. Effect of ionic liquid/organic solvent pretreatment on the enzymatic hydrolysis of corncob for bioethanol production. Part 1: Structural characterization of the lignins. *Ind. Crops Prod.* **2013**, *43*, 570–577. [[CrossRef](#)]
33. Jääskeläinen, A.S.; Sun, Y.; Argyropoulos, D.S.; Tamminen, T.; Hortling, B. The effect of isolation method on the chemical structure of residual lignin. *Wood Sci. Technol.* **2003**, *37*, 91–102. [[CrossRef](#)]
34. Long, J.; Li, X.; Guo, B.; Wang, F.; Yu, Y.; Wang, L. Simultaneous delignification and selective catalytic transformation of agricultural lignocellulose in cooperative ionic liquid pairs. *Green Chem.* **2012**, *14*, 1935–1941. [[CrossRef](#)]
35. Liu, J.; Qi, L.; Yang, G.; Xue, Y.; He, M.; Lucia, L.A.; Chen, J. Enhancement of Lignin Extraction of Poplar by Treatment of Deep Eutectic Solvent with Low Halogen Content. *Polymers* **2020**, *12*, 1599. [[CrossRef](#)] [[PubMed](#)]
36. Zhao, X.B.; Wang, L.; Liu, D.H. Peracetic acid pretreatment of sugarcane bagasse for enzymatic hydrolysis: A continued work. *J. Chem. Technol. Biotechnol.* **2010**, *83*, 950–956. [[CrossRef](#)]
37. Wen, J.L.; Sun, S.L.; Yuan, T.Q.; Sun, R.C. Structural elucidation of whole lignin from Eucalyptus based on preswelling and enzymatic hydrolysis. *Green Chem.* **2015**, *17*, 1589–1596. [[CrossRef](#)]
38. Del Río, J.C.; Rencoret, J.; Prinsen, P.; Martínez, A.T.; Ralph, J.; Gutiérrez, A. Structural Characterization of Wheat Straw Lignin as Revealed by Analytical Pyrolysis, 2D-NMR, and Reductive Cleavage Methods. *J. Agric. Food Chem.* **2012**, *60*, 5922–5935. [[CrossRef](#)]

39. Miles-Barrett, D.M.; Neal, A.R.; Hand, C.; Montgomery, J.R.; Panovic, I.; Ojo, O.S.; Lancefield, C.S.; Cordes, D.B.; Slawin, A.M.; Lebl, T.; et al. The synthesis and analysis of lignin-bound Hibbert ketone structures in technical lignins. *Org. Biomol. Chem.* **2016**, *14*, 10023–10030. [[CrossRef](#)]
40. Lyu, G.; Li, T.; Ji, X.; Yang, G.; Liu, Y.; Lucia, L.; Chen, J. Characterization of Lignin Extracted from Willow by Deep Eutectic Solvent Treatments. *Polymers* **2018**, *10*, 869. [[CrossRef](#)] [[PubMed](#)]
41. Lourenço, A.; Rencoret, J.; Chemetova, C.; Gominho, J.; Gutiérrez, A.; Pereira, H.; José, C. Isolation and Structural Characterization of Lignin from Cardoon (*Cynara cardunculus* L.) Stalks. *BioEnergy Res.* **2015**, *8*, 1946–1955. [[CrossRef](#)]
42. Del Río, J.C.; Prinsen, P.; Rencoret, J.; Nieto, L.; Jiménez-Barbero, J.; Ralph, J.; Martínez, A.T.; Gutiérrez, A. Structural characterization of the lignin in the cortex and pith of elephant grass (*Pennisetum purpureum*) stems. *J. Agric. Food Chem.* **2012**, *60*, 3619. [[CrossRef](#)]
43. Azarpira, A.; Ralph, J.; Lu, F. Catalytic Alkaline Oxidation of Lignin and its Model Compounds: A Pathway to Aromatic Biochemicals. *BioEnergy Res.* **2014**, *7*, 78–86. [[CrossRef](#)]
44. Abednatanzi, S.; Abbasi, A.; Masteri-Farahani, M. Immobilization of catalytically active polyoxotungstate into ionic liquid-modified MIL-100(Fe): A recyclable catalyst for selective oxidation of benzyl alcohol. *Catal. Commun.* **2017**, *96*, 6–10. [[CrossRef](#)]
45. Tsigdinos, G.A. Heteropoly compounds of molybdenum and tungsten. In *Topics in Current Chemistry*; Springer: Berlin/Heidelberg, Germany, 1978; Volume 76, pp. 1–64.
46. Evtuguin, D.V.; Neto, C.P.; Rocha, J. Lignin Degradation in Oxygen Delignification Catalysed by  $[\text{PMo}_7\text{V}_5\text{O}_{40}]^{8-}$  Polyanion. Part. I. Study on Wood Lignin. *Holzforschung* **2000**, *54*, 381–389. [[CrossRef](#)]